Earth and Planetary Science Letters 411 (2015) 199–207

Contents lists available at ScienceDirect

Earth and Planetary Science Letters

www.elsevier.com/locate/epsl

Catastrophic emplacement of giant landslides aided by thermal decomposition: Heart Mountain, Wyoming

Thomas M. Mitchell [a,b,*], Steven A.F. Smith [b,c], Mark H. Anders [d], Giulio Di Toro [b,e], Stefan Nielsen [f], Andrea Cavallo [b], Andrew D. Beard [g]

[a] Department of Earth Sciences, University College London, Gower Street, London, UK
[b] Istituto Nazionale di Geofisica e Vulcanologia, Roma, Italy
[c] Department of Geology, University of Otago, Dunedin, 9054, New Zealand
[d] Department of Earth and Environmental Sciences and Lamont-Doherty Earth Observatory, Columbia University, Palisades, NY 10964, United States
[e] Dipartimento di Geoscienze, Università di Padova, Padova, Italy
[f] Earth Sciences Department, University of Durham, South Road, DH1 3LE, UK
[g] Department of Earth and Planetary Sciences, Birkbeck, University of London, Malet Street, London, WC1E 7HX, UK

ARTICLE INFO

Article history:
Received 9 June 2014
Received in revised form 18 October 2014
Accepted 21 October 2014
Available online 23 December 2014
Editor: P. Shearer

Keywords:
landslide
thermal decomposition
Heart Mountain
thermal pressurization
high velocity friction

ABSTRACT

The Heart Mountain landslide of northwest Wyoming is the largest known sub-aerial landslide on Earth. During its emplacement more than 2000 km^3 of Paleozoic sedimentary and Eocene volcanic rocks slid >45 km on a basal detachment surface dipping 2°, leading to 100 yr of debate regarding the emplacement mechanisms. Recently, emplacement by catastrophic sliding has been favored, but experimental evidence in support of this is lacking. Here we show in friction experiments on carbonate rocks taken from the landslide that at slip velocities of several meters per second CO_2 starts to degas due to thermal decomposition induced by flash heating after only a few hundred microns of slip. This is associated with the formation of vesicular degassing rims in dolomite clasts and a crystalline calcite cement that closely resemble microstructures in the basal slip zone of the natural landslide. Our experimental results are consistent with an emplacement mechanism whereby catastrophic slip was aided by carbonate decomposition and release of CO_2, allowing the huge upper plate rock mass to slide over a 'cushion' of pressurized material.

1. Introduction

In the early 1900s, a low-angle detachment was recognized at Heart Mountain and initially attributed to thrusting of Paleozoic rocks onto Eocene rocks (Dake, 1916). In the 1940s the detachment was shown to be a landslide (Bucher, 1947), and in the late 1950s and early 1960s its enormous areal extent (Fig. 1, Fig. 2a) was first established (Hauge, 1985, 1990, 1993). Since then, debate has centered on whether emplacement was catastrophic (Anders et al., 2011; Beutner and Gerbi, 2005; Beutner and Hauge, 2009; Craddock et al., 2000, 2009; Pierce, 1960, 1973; Voight, 1973) or incremental (Hauge, 1985) and by which mechanisms such a massive volume of upper plate rock could have moved across a basal surface with an average regional dip of only 2° (Anders et al., 2011; Craddock et al., 2000; Hughes, 1970; Melosh, 1983). Central to the debate is the character of deformation at the landslides base (Anders et al., 2010; Beutner and Craven, 1996; Craddock et al., 2009; Hauge, 1990). Consensus amongst workers today is that emplacement was catastrophic, taking on the order of minutes to hours, and that initial movement of the landslide was triggered by Eocene volcanic activity (Aharonov and Anders, 2006; Anders et al., 2010; Beutner and Craven, 1996; Craddock et al., 2009; Goren et al., 2010a, 2010b; Hughes, 1970; Malone et al., 2014; Melosh, 1983).

Although long-runout landslides are known to occur on high-angle surfaces (e.g. Brian Dade and Huppert, 1998), one of the long-standing paradoxes in geomechanics is how large landslides are able to move great distances on low-angle surfaces when frictional resistance demands that they not. There have been a number of hypotheses to explain this phenomenon (e.g. Pudasaini and Miller, 2013 and references therein), but almost no empirical data to support one model over another. Suggested mechanisms to account for the >45 km long runout

* Corresponding author.
E-mail address: tom.mitchell@ucl.ac.uk (T.M. Mitchell).

http://dx.doi.org/10.1016/j.epsl.2014.10.051

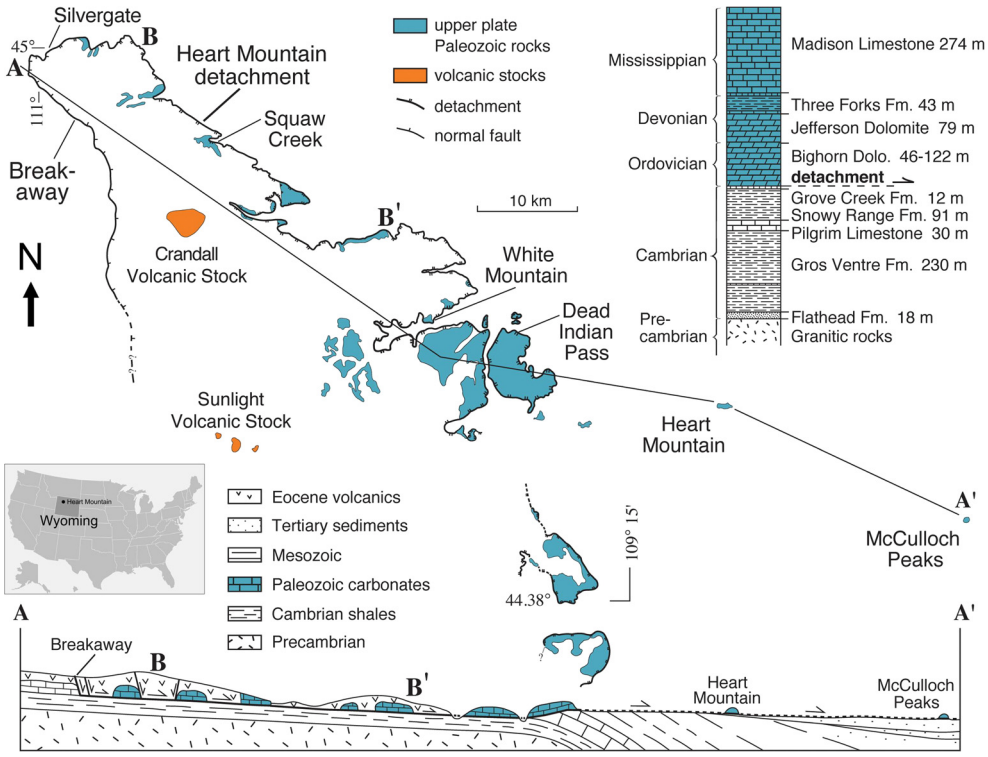

Fig. 1. Map of the Heart Mountain slide block located in northwestern Wyoming and southeastern Montana, showing the sampling areas referred to in the text. Modified from Anders et al. (2010).

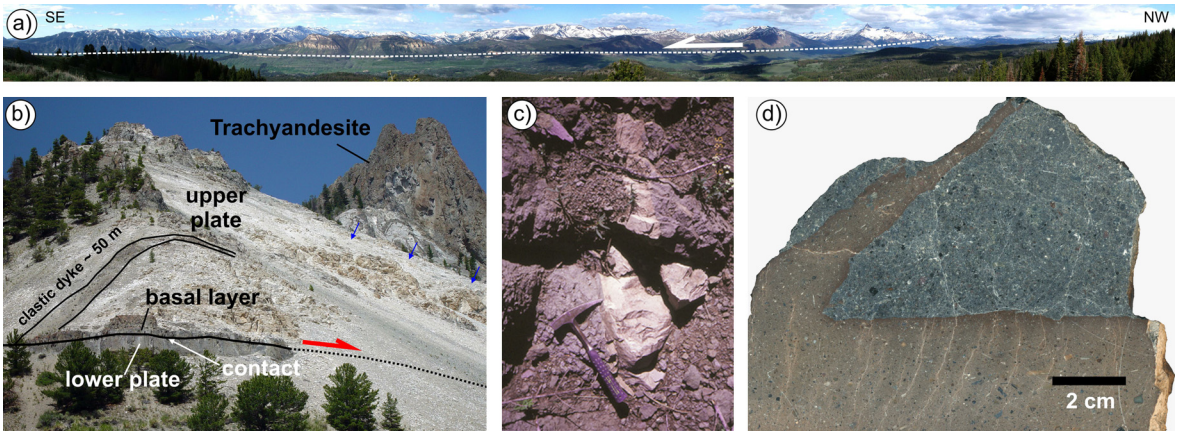

Fig. 2. (a) Photograph of ~30 km of the Heart Mountain slide block (B to B′ in Fig. 1). View looking southwest from south flank of the Beartooth Mountains. Photograph is by Anna Foster with her permission. (b) White Mountain sampling site. White rocks are upper plate marbleized Ordovician Bighorn Dolomite and Mississippian Madison Limestone. The gray horizontal layer is the ~3 m-thick basal layer overlying a thin sliver of the lower plate Bighorn Dolomite and Cambrian Snowy Range Formation. The dark trachyandesite peak in the upper right is an Eocene stock of the Absaroka Group Volcanics. Marbleization is due to stock igneous intrusion prior to slide emplacement. Modified from Anders et al. (2010). (c) A clastic dike/injectite at Silvergate, Montana (light colored injectite is intruded into dark Eocene Absaroka Volcanic rocks). This dike is located within a meter of the basal contact. At this location carbonized Eocene wood was found in the dike (see Anders et al., 2010, their Fig. 3f). (d) Cut slab of clastic dike/injectite from Silvergate, Montana location.

of the Heart Mountain landslide include hydroplaning on cognate waters (Voight, 1973), injection of pressurized volcanic gases at the slide's base (Beutner and Gerbi, 2005; Hughes, 1970), earthquake acoustic fluidization (Melosh, 1983), granular dynamic fluidization (Anders et al., 2000), hydrothermal overpressuring (Aharonov and Anders, 2006; Goren et al., 2010a, 2010b) and, more recently, overpressuring from generation of CO_2 gas caused by thermal decomposition of the basal carbonates (Anders et al., 2010; Beutner and Gerbi, 2005).

Here we present experimental results that support the unique role of carbonate decomposition in the long-runout of large terrestrial landslides. We show that hypotheses of landslide fluidization by CO_2 gas generation, hitherto speculated at, are well supported by a combination of our experimental results and field observations.

2. Natural observations

One of the best exposures of the basal section of the HM landslide is at White Mountain (Figs. 1, 2b). At this locality a Paleozoic section of marbleized Ordovician Bighorn Dolomite to Mississippian Madison Limestone in the upper plate was emplaced (Fig. 1)

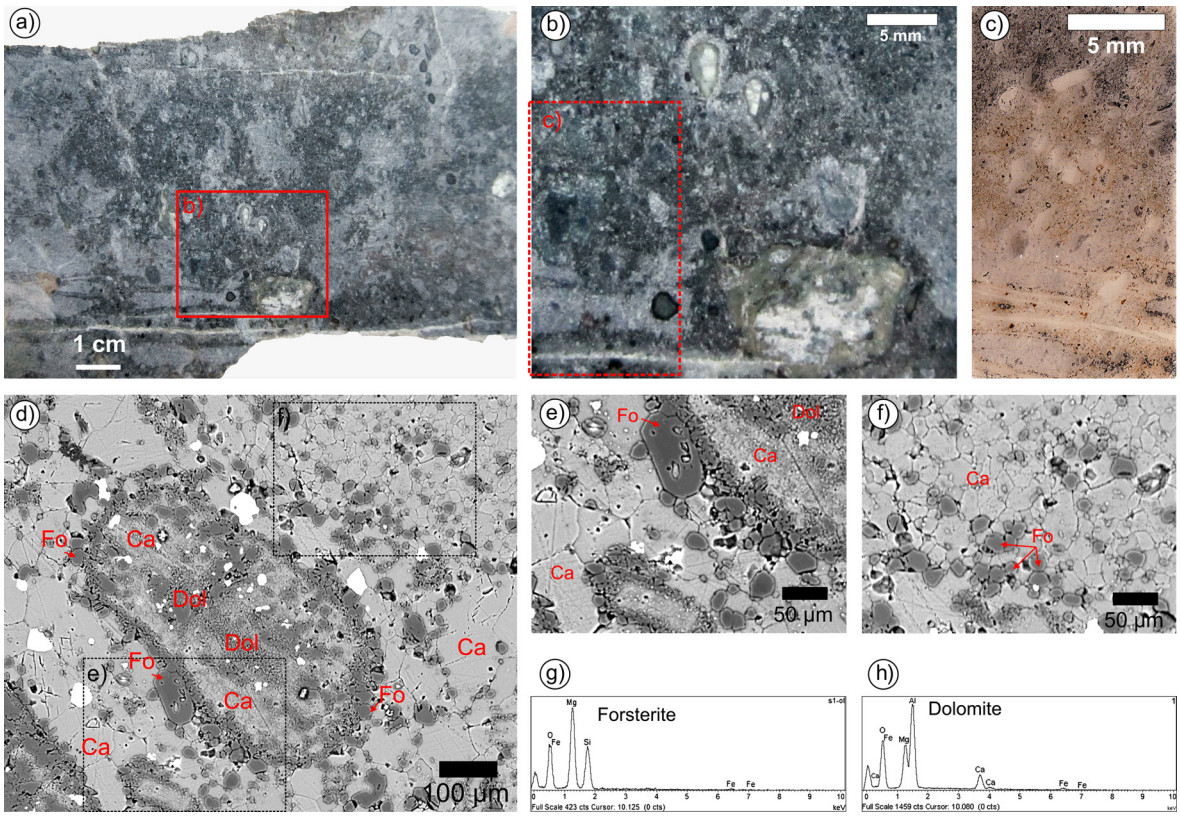

Fig. 3. (a) Polished slab of basal section from the White Mountain, cut parallel to the slip direction. Large angular clasts of carbonates and volcanic material up to 1 cm can be seen within a microcrystalline matrix. (b) Expanded view of (a) showing location of thin section. (c) Reflected light scan of thin section of basal section matrix material. (d) Dolomite clast containing a concentric layer of calcite up to 100 µm wide within a calcite matrix. (e) Higher magnification of calcite rim showing mottled texture and irregular margins, with aggregates of much smaller grains of forsterite on the outer boundary. (f) Higher magnification of calcite matrix showing euhedral grains of forsterite. (g) Typical EDS spectrum showing a pure forsterite composition. (h) EDS spectrum showing dolomite. Note that spikes in O and Al are due to nanograins of alumina polish (Al_2O_3) on thin sections.

onto Bighorn Dolomite and mudstones of the Cambrian Snowy Range Formation in the lower plate. The basal slip layer at this locality is up to 3.5 m thick and lies above an irregular contact that delimits the top of the lower plate. Clastic dykes that have previously been interpreted as injectites (Anders et al., 2010; Craddock et al., 2012) are commonly found originating within the basal slip layer and extending sub-vertically into the upper plate (Fig. 2b–d) for distances of up to 120 m (Anders et al., 2010; Craddock et al., 2012). The composition of the basal slip layer varies considerably along the length of the landslide depending on local protolith, but a significant proportion of carbonate material is generally found at every location previously examined (Anders et al., 2010). At White Mountain it comprises millimeter to centimeter sized well-rounded clasts of limestone and dolomite both ranging from 20–100 µm in diameter, less abundant angular fragments of volcanic glass up to 1 cm in diameter, and other types of volcanic clast suspended in a microcrystalline carbonate matrix (Fig. 3a–d).

Field-emission scanning electron microscope (SEM) and Energy-Dispersive X-Ray spectroscopy (EDS) observations indicate that the carbonate matrix is predominantly composed of calcite grains 50–100 µm in size displaying well-defined "polygonal" grain shapes, with grain boundaries regularly forming triple junctions (Fig. 3d–f). Dolomite clasts dispersed throughout the matrix contain an outer concentric layer up to 100 µm wide of fine-grained (<5 µm) mottled calcite (up to 70% of the entire clast) (Fig. 3d, e). The margins of the concentric layer of calcite are highly irregular and in places the calcite are observed to infill cracks within the large dolomite grain core, indicating that it may be a secondary generation of calcite (Fig. 3e). On the outer boundary of the dolomite grains, aggregates of much smaller euhedral tabular grains (<10 µm in size) are commonly found (Fig. 3d, e). EDS analysis shows that many of these grains are composed of pure forsterite (Fig. 3d–g). Although previously identified (Anders et al., 2010), there was no direct evidence that forsterite was generated during the sliding and that it might be associated with the decarbonation of dolomite. However, here we found near-perfect basal sections (Fig. 3e) suggesting the forsterite grains may have grown in-situ on the rims of the dolomite grains. Euhedral grains of forsterite <10 µm in size are also found distributed throughout the calcite matrix, commonly located at grain triple junctions (Fig. 3e). Where forsterite grains have higher density within the matrix, calcite grains tend to be significantly reduced in size, suggesting pinning may locally restrict the calcite grain growth (e.g. Herwegh et al., 2008) and that both calcite and forsterite growth are synchronous.

3. Experimental methods

In an attempt to reproduce some of the distinct microstructures seen in the basal slip zone of the landslide at White Mountain, we performed ten low-to-high velocity friction experiments on powdered carbonate rocks collected from the landslide. The carbonates were sheared using a sample holder for incohesive rocks within SHIVA (slow- to high-velocity rotary-shear friction apparatus) at the Istituto Nazionale di Geofisica e Vulcanologia (INGV), Rome, Italy (Di Toro et al., 2010; Smith et al., 2013). Powders were prepared by crushing and sieving (to a particle size of <250 µm) initially intact host rocks of Madison Limestone and

Bighorn Dolomite collected from White Mountain (Figs. 1a, 2b). As the basal layer of the landslide at this locality is composed of comminuted pieces of both the upper and lower plates, three types of gouge were used in the experiments; two end members of 100 wt% Bighorn Dolomite and 100 wt% Madison Limestone, and an intermediate mix of 50 wt% dolomite and 50 wt% limestone. Powdered samples were sheared for up to 3 m displacement at velocities between 0.01 $m\,s^{-1}$ and 1 $m\,s^{-1}$ at constant normal stresses up to 10 MPa, corresponding to a depth of around 450 m. Normal stresses were limited in this case due to minor gouge extrusion at displacements approaching 3 m. Previous estimates put the upper plate thickness at 2–4 km prior to landslide motion (Aharonov and Anders, 2006), so our results should be considered as a lower bound for representing conditions during the movement phase. Experiments were performed in a closed environmental chamber containing a mass spectrometer to detect CO_2 output during the experiments (Smith et al., 2013; Violay et al., 2013). CO_2 gas emission was monitored using an OmniStar™ GSD 301 O mass spectrometer, for general gas analysis at atmosphere pressure. The experimentally deformed gouges were recovered and impregnated with epoxy, and thin sections were cut perpendicular to the gouge layers and approximately parallel to the slip direction to conduct geochemical and microstructural investigations. A JEOL 6500 field-emission scanning electron microscope at the Istituto Nazionale di Geofisica e Vulcanologia (Rome) was used to image microstructures. Chemical analysis was carried out using a JEOL JXA8100 Superprobe with an Oxford Instruments INCA system (EDS) and an accelerating voltage of 15 kV, current of 1 μA and a beam diameter of 1 μm.

4. Results

Four representative experiments are shown in Fig. 4a. At a slip rate of 0.01 $m\,s^{-1}$, the friction coefficient (μ, shear stress divided by normal stress) remained high during the experiments (s638, $\mu = 0.7$–0.8, Fig. 4a) and no CO_2 output was detected (Fig. 4b). At slip rates of 1 $m\,s^{-1}$, all three gouge types (pure calcite, pure dolomite, 50/50 dol./cal.) show peak friction coefficients of ~0.6 followed by dynamic weakening to reach minimum friction coefficients as low as 0.25 (Fig. 4a). This was broadly concomitant with a pronounced spike in CO_2 emissions (increasing from background levels in the lab. of 360–385 ppm to maximum values of 3580 ppm) that were registered by the mass spectrometer within 6–10 seconds of slip initiation (Fig. 4b).

Two very low-displacement tests (8.5 mm and 0.1 mm) were performed to constrain whether CO_2 is generated during the earliest stages of slip (Fig. 5). The target slip velocity in these experiments was 6.5 $m\,s^{-1}$ but because the displacements were so small, the peak velocities reached (with acceleration and deceleration rates of 90 $m\,s^{-2}$) were ca. 0.7 $m\,s^{-1}$ (for the 8.5 mm test; Fig. 5a) and ca. 0.06 $m\,s^{-1}$ (for the 0.1 mm test; Fig. 5b). For 8.5 mm of total slip, a significant increase of around 80 ppm CO_2 was detected above background variations (360–385 ppm), and for just 0.1 mm of total slip a smaller increase of up to 20 ppm was detected (Fig. 5c).

4.1. Microstructural observations

Microstructural observations indicate that displacement at slip rates of 0.01 $m\,s^{-1}$ was accommodated by distributed cataclastic deformation (Fig. 6), formation of Riedel shears (primarily of R'-type following Logan et al., 1979) and grain size reduction across the entire 1 mm thick gouge layer. Dolomite and calcite grains deformed at this slip rate are typically rounded and range in size from several hundred nm to 20 μm (Fig. 6b, c). Longer

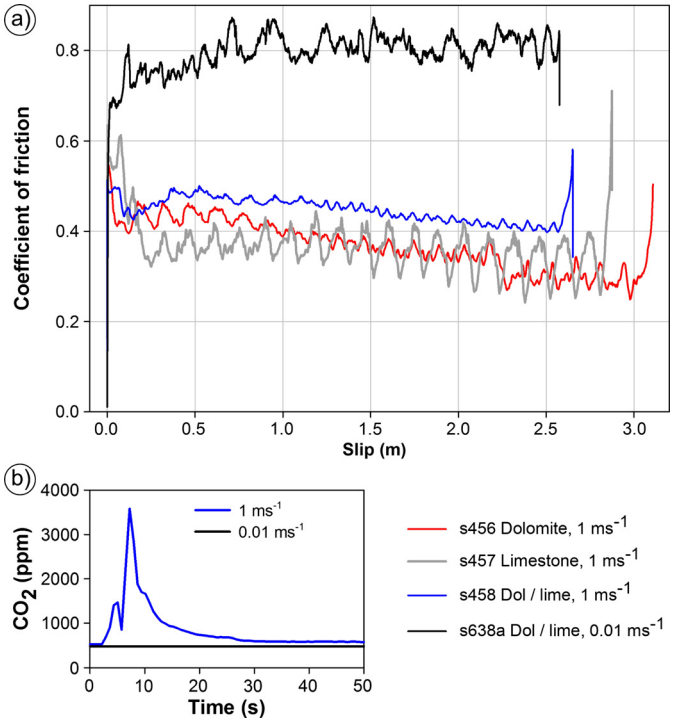

Fig. 4. Mechanical data and microstructures from friction experiments. (a) Friction coefficient vs displacement for four representative experiments in dolomite, limestone and dolomite/limestone 50/50 mixes. (b) CO_2 output versus time for experiments s458 and s638a run at 1 $m\,s^{-1}$ and 0.01 $m\,s^{-1}$ respectively. Experiment begins at 0 s.

displacement (3–5 m) experiments conducted on mixed dolomite–calcite gouges at slip rates of 1 $m\,s^{-1}$ reveal localization of deformation to a fine-grained principal slip zone (PSZ) ~10 μm thick (Fig. 7a, b) defined by a marked reduction in grain size compared to the bulk gouge layer (Fig. 7b, e, f). Secondary SEM observations of the discrete principal slip surface cutting the PSZ show small (<500 nm in size), tightly-packed and polygonal calcite grains that form a surface "pavement" with negligible porosity (Fig. 7h). Adjacent to the PSZ is a layer ~100 μm thick (Fig. 7a, b) in which the overall size and distribution of dolomite clasts is similar to that in the starting materials, indicating that the layer was not highly strained. However, the layer contains two distinct microstructures not found elsewhere in the gouge layers; (1) a crystalline calcite matrix showing roughly polygonal, interlocking calcite grains <10 μm in size (Fig. 7c, d, g) and (2) dolomite grains containing vesicular rims and planar trails of vesicles (Fig. 7c, d, g), typical of decarbonation. We refer to this zone as the decarbonated dolomite zone (DDZ). All of the dolomite clasts within the DDZ have outer rims with a vesicular texture. The Mg content in dolomite clasts increases towards the principal slip zone (Fig. 7b, Fig. 8) indicating a gradient in both temperature and the amount of decarbonated material. In the DDZ adjacent to the principal slip zone the dolomite clasts are often completely engulfed by the vesicular texture, forming highly porous grains surrounded by the crystalline calcite matrix (Fig. 7c, d).

4.2. Estimates of temperature increase within experimental slip zones

To estimate the temperature distribution across the gouge layer produced by frictional heat diffusing away from the principal slip surface in experiment s458, we calculated the temperature increase ΔT with time within the 10 μm thick experimental PSZ and adjacent gouge layer using a simplified solution for heat wave propagation in one dimension which accounts for heat loss during

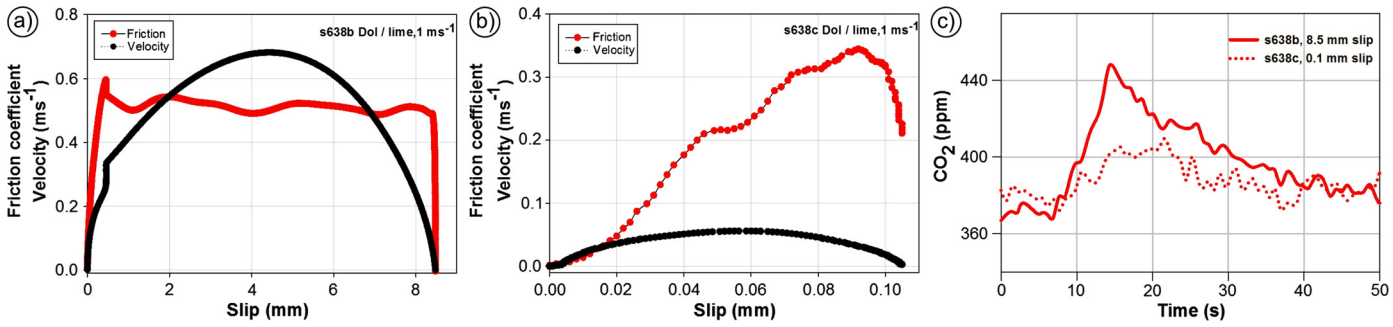

Fig. 5. Velocity profiles for short displacement experiments, using the maximum SHIVA acceleration and deceleration rates of 90 $m\,s^{-2}$. (a) Experiment s638b with a total displacement of 8.5 mm, reaching a peak velocity of 0.7 $m\,s^{-1}$. Peak friction of 0.6 is achieved at 0.45 mm displacement, followed by the onset of dynamic weakening at a velocity of 0.43 $m\,s^{-1}$. (b) Experiment s638c with a total displacement of 0.1 mm, reaching a peak velocity of 0.06 $m\,s^{-1}$. Peak friction seen is not achieved due to deceleration initiating when friction has risen to just 0.22 during the initial strengthening. (c) CO_2 output versus time for experiments s638b and s638c with short displacements. Experiments begin at 0 s.

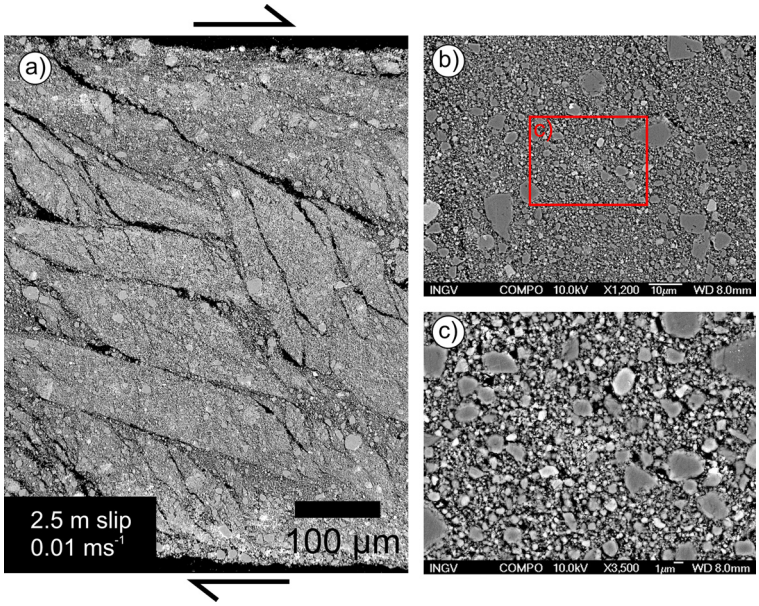

Fig. 6. (a) Back Scattered Scanning Electron Microscope (BSSEM) images of microstructures representative of 2.5 m of slip at 0.01 $m\,s^{-1}$ showing cataclasis and distributed deformation in experiment s638a. (b) and (c) show magnifications of fine grained comminuted material.

the endothermic decarbonation reaction (Brantut et al., 2011; Sulem and Famin, 2009). Temperature is estimated by solving the one dimensional heat diffusion equation in the presence of a heat source rate $\tau(t)V(t)$ (frictional power, where V = slip rate, and τ = shear stress) and a heat sink rate $\phi(t)$ due to the latent heat of decarbonation of dolomite and calcite. Experiments described in our study demonstrate that decomposition occurs within a zone c. 100 µm wide. The net heat rate available at any given time t is hence:

$$\tau(t)V(t) - \phi(t)$$

The temperature increase $\Delta T(t,x)$ within the experimental slip zone is estimated using the classical solution for 1D diffusion with imposed heat flow at the boundary (Carslaw and Jaeger, 1959). Assuming frictional power is generated within a very thin slip zone (we neglect the initial strain localization phase):

$$\Delta T(x,t) = \frac{1}{2\rho c\sqrt{\kappa\pi}} \int_0^t \frac{\tau(t')V(t') - \phi(t')}{\sqrt{t-t'}} e^{\frac{-x^2}{4\kappa(t-t')}} dt' \qquad (1)$$

where x is the distance away from the slip zone, $\rho = 2800\ kg\,m^{-3}$ is mass density, $\kappa = 1.74 \times 10^{-6}\ m^2\,s^{-1}$ is thermal diffusivity and $c = 845\ J\,kg^{-1}\,K^{-1}$ is heat capacity (these values are obtained by computing the harmonic mean of the values of dolomite and calcite from Di Toro et al., 2011).

4.2.1. Case with no heat sinks, i.e., $\phi = 0$

This provides an upper bound for the temperature on the sliding surface, as no heat sinks have been included other than diffusion. In this case the bulk decarbonation temperature for dolomite, ~600 °C (De Paola et al., 2011b; Fondriest et al., 2013), is reached at around 75 cm of slip (Fig. 9a). Release of CO_2 detected for slips as small as 0.1 and 0.85 mm in the experiments (Fig. 5c) is probably due to grain crushing inducing localized high temperatures by flash heating, while the bulk temperature of the sliding interface is still much lower. According to the relatively high temperatures obtained without heat sinks, decarbonation should have occurred up to about 500 µm from the slip zone, during the last half-second of slip. However, microstructural observations show that decomposition occurred only within about 100 µm of the slip zone (Fig. 8). We try to match this experimental observation by including a heat sink due to the latent heat of decarbonation.

4.2.2. Case with heat sink due to decarbonation

Here we account for the heat loss by decarbonation. For simplicity, we assume a priori that such a heat sink is consistent in the region immediately adjacent to the slip zone, and consider

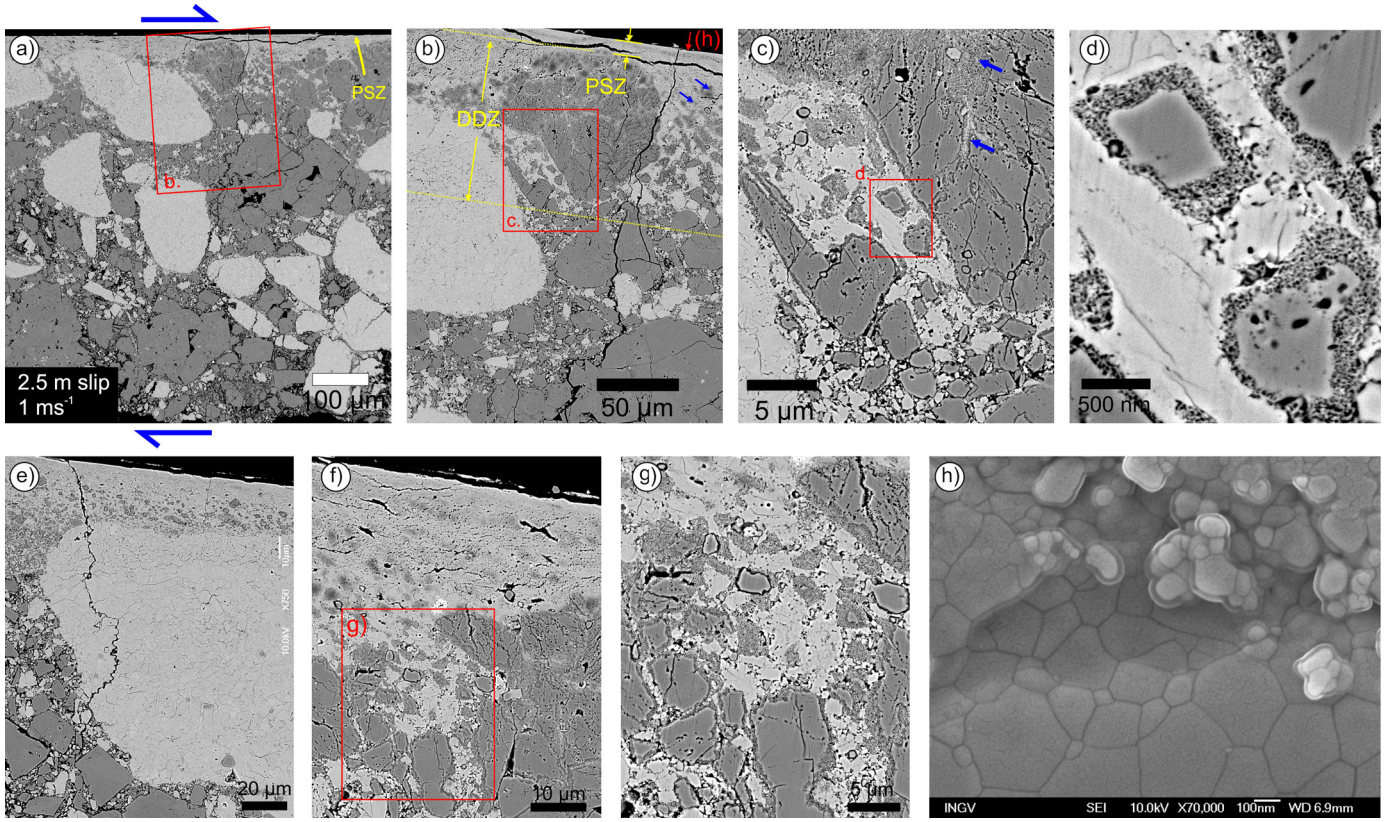

Fig. 7. (a) BSSEM images of microstructures representative of 2.5 m of slip at 1 m s^{-1} showing localization of deformation to a Principal Slip Zone (PSZ) in experiment s458. Outside the PSZ, dolomite and calcite grains are relatively undeformed, with grain sizes close to those of the starting material. (b) Expanded view of microstructures within (a) (experiment s458). Dark gray is dolomite, white is calcite. Blue arrows denote 'ghost' decarbonated clasts. PSZ denotes the principal slip zone, and DDZ the dolomite decarbonated zone. (c) and (d) show zooms from (b), showing dolomite clasts with vesicular decarbonation rims suspended in a calcite matrix, with blue arrows denoting decarbonation networks in larger dolomite grains. (e) shows a large intact calcite clast within the DDZ, showing a lack of significant shear outside of the PSZ. (f) Boundary between the PSZ and DDZ, showing intense vesiculation closest to the PSZ. (g) Expanded view of (f) showing VDRs which increase in thickness closes to the PSZ. (h) Secondary Electron Scanning Electron Microscope image showing a view perpendicular to the slip surface. (For interpretation of the references to color in this figure legend, the reader is referred to the web version of this article.)

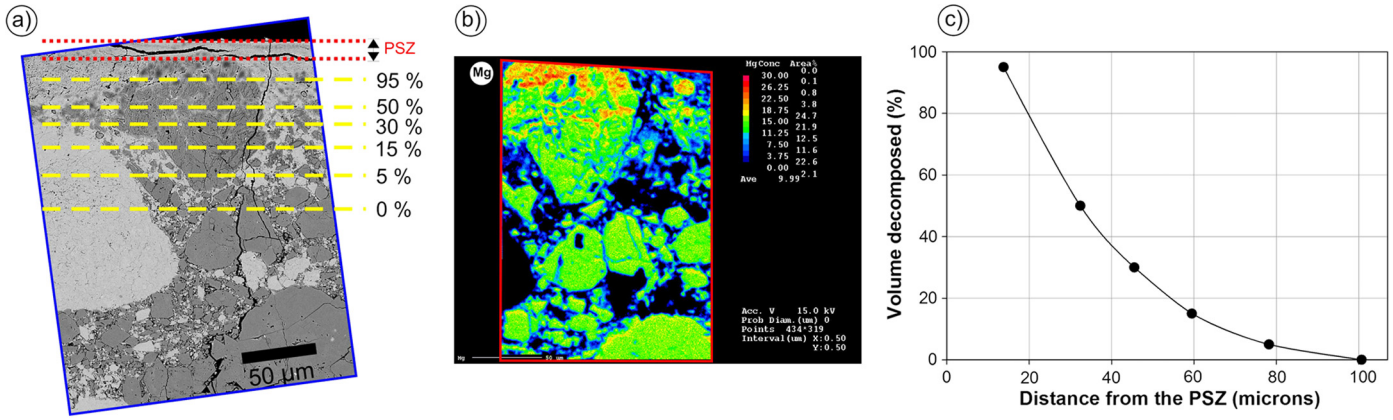

Fig. 8. (a) Estimate of percentage of decarbonated material indicated by the amount of vesiculation in Fig. 7b within a dolomite grain relative to intact grain (e.g. Fig. 7d). Percentages are an average value from the analysis of 5 dolomite grains along each yellow scanline. (b) Electron Microprobe chemical analysis of Fig. 7b showing relative concentrations of Mg on the edges of the large dolomite clast within the DDZ which likely indicates a decarbonation reaction product. (c) Percentage of decarbonated material plotted as a function of distance from the PSZ. (For interpretation of the references to color in this figure legend, the reader is referred to the web version of this article.)

that both the main frictional heat sources and heat sinks are located within a layer of negligible thickness so that we can locate the net heat source on the plane $x = 0$ at the center of the PSZ for the solution of the problem. This approximation is justified by the experimental observation that only negligible reactions took place outside a region 100 µm thick adjacent to the principal slip surface.

We assume an Arrhenius thermal dependence of the reaction kinetics. We compute the rate of mass decomposed as a function of time and the corresponding rate of heat loss. After Sulem and Famin (2009), we express the reaction rate (in mass per unit volume m per unit time t) as:

$$\frac{\partial m}{\partial t} = \alpha\big(1 - n(t)\big)\rho A \mathrm{Exp}\left[\frac{-E_a}{(RT(t))}\right] \tag{2}$$

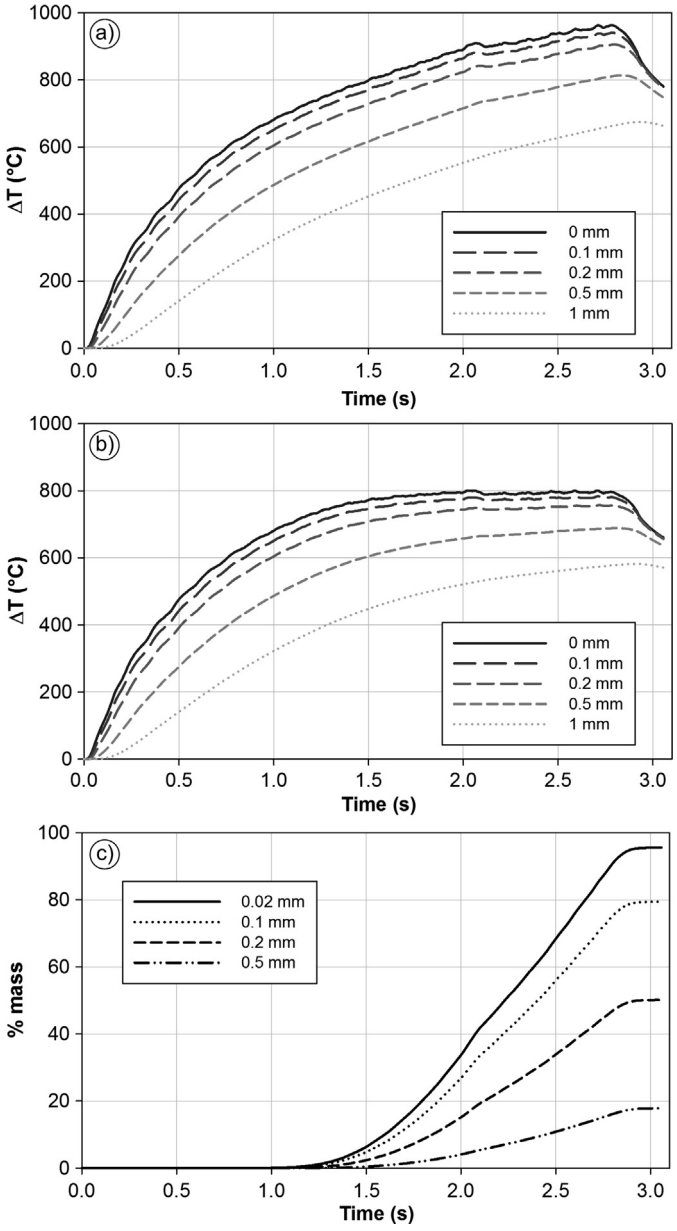

Fig. 9. (a) Temperature increase as a function of time in the absence of heat sinks, calculated for distances of 0, 0.1, 0.2, 0.5, and 1 mm from the PSZ. Solid curve (0 mm) corresponds to the center of the slip zone. (b) Temperature increase as a function of time, in the presence of heat sink due to decarbonation over a thickness of 0.1 mm, calculated for distances of 0, 0.1, 0.2, 0.5, and 1 mm from the PSZ. Note the clear "thermal buffering effect" of the reaction. (c) Proportion of decarbonated mass at distances from the PSZ of $x = 0.02, 0.1, 0.2$ and 0.5 mm from the computation including heat sinks.

where $R = 8.31\ \mathrm{J K^{-1} mol^{-1}}$ is the gas constant, $E_a = 319 \times 10^3\ \mathrm{J mol^{-1}}$ is the activation energy and $A = 2.95 \times 10^{15}\ \mathrm{s^{-1}}$ is the pre-exponential factor. For simplicity, we assume that all forms of decarbonation of calcite and dolomite will not differ significantly in their energy absorption and describe a single reaction with the above values of E_a and A, and $L = 3190 \times 10^3\ \mathrm{J kg^{-1}}$ for latent heat (Sulem and Famin, 2009). $n(t)$ is the proportion of carbonated material which has been decarbonated at time t and α is the initial fraction of carbonated material in the bulk rock which we approximate by $\alpha = 1$.

We may write the heat sink rate per unit fault area and the proportion of mass loss per unit time per unit fault area, respectively, as:

$$\phi(t) = hL\frac{\partial m}{\partial t} \tag{3}$$

$$\frac{\partial n}{\partial t} = \frac{1}{\rho\alpha}\frac{\partial m}{\partial t} \tag{4}$$

The larger the thickness h of rock affected by decarbonation around the slip zone, the smaller the net heat and its penetration distance. Different values of h were tested for consistency: the penetration distance of the 600 °C isotherm resulting from the computation should be close to the h value used in the computation. For a layer of about $h = 130$ µm around the slip zone, we do obtain a heat penetration of the same order (see Fig. 9b). Such a value is also consistent with the microstructural observations. Fig. 9b shows a clear "thermal buffering effect" of the reaction, as noted in Sulem and Famin (2009) and Brantut et al. (2011), which starts when temperatures approach 600 °C (decarbonation triggering) and is fully effective at about 800 °C where decarbonation is fast.

Inserting the value of ϕ (3) into (1) and solving iteratively in time, we obtain the temperature and the percentage of decarbonated volume at different distances from the PSZ as indicated in Fig. 9c from the computation including heat sinks. At the end of the experiment, 80% of the mass is decarbonated at distances of $x = 0.1$ mm while the percentage drops rapidly thereafter to around ~25% at $x = 0.5$ mm. A distance of 0.1 mm corresponds to a thickness of 0.2 mm, which is roughly compatible with the slightly smaller h value adopted in the computation (0.13 mm).

5. Discussion

We suggest that the microstructures within the ~100 µm-thick DDZ adjacent to the principal slip zone are the result of thermal decomposition (e.g. Han et al., 2007a, 2007b) in the case of the vesicular rims in dolomite grains, and recrystallization in the case of the crystalline calcite matrix (Smith et al., 2013), both caused by the frictional heat generated within the 10 µm thick PSZ during localized shear and diffusing into the adjacent material. Similar vesicular decarbonation rims (VDRs) have been observed in rapidly heated and decomposed carbonates trapped in volcanic magmas (Deegan et al., 2010) and in calcite grains found in the PSZs of large-displacement thrust faults (Collettini et al., 2013). Electron Microprobe chemical analysis shows increased concentrations of Mg on the edges of the large dolomite clast within the DDZ closest to the PSZ (Fig. 8b) which likely indicates a decarbonation reaction product. Temperature calculations show that at the end of experiment s458 (1 $\mathrm{m\,s^{-1}}$, 50% dolomite/50% limestone) 80% of the mass within 100 µm of the principal slip surface has decarbonated, while the percentage drops rapidly at greater distances. This is broadly consistent with microstructural observations showing that the width of the DDZ where vesicular rims are present is ca. 100 µm (Figs. 7b, 8).

The lack of significant grain size reduction or shear offset in the dolomite and calcite grains outside the PSZ (Fig. 7a–b, f–g) but within the DDZ suggests that no significant displacements were hosted outside of the PSZ, and heat was likely generated within the PSZ due to extreme localization of strain, and diffused away from the slip surface decarbonating the dolomite grains. Evidence of degassing in the very small-displacement experiments indicates that CO_2 starts to be liberated almost immediately after the onset of shearing. Temperature calculations suggest that the bulk temperature needed to initiate decarbonation of dolomite (600 °C) is only reached after around 75 cm of slip in these experiments (Fig. 9). This indicates that the early release of CO_2 (detected for slips as small as 0.14 mm in the experiments) is likely due to grain crushing and flash heating at grain–grain contacts (Beeler et al., 2008; Goldsby and Tullis, 2011; Proctor et al., 2014;

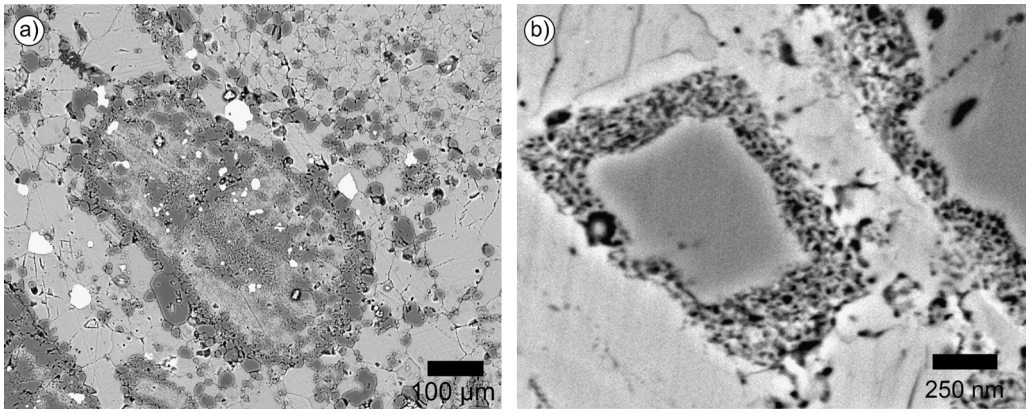

Fig. 10. Comparison of natural dolomite clast (Fig. 3d) containing a concentric layer of calcite up to 100 µm wide within a calcite matrix, and experimentally produced dolomite clasts (Fig. 7d) with vesicular decarbonation rims suspended in a calcite matrix. Experimental dolomite clasts are smaller due to initial gouge being prepared to a grain size of <250 µm.

Rice, 2006; Tisato et al., 2012) inducing localized high temperatures and subsequent decarbonation (e.g. De Paola et al., 2011a, 2011b). In the calcite matrix, no textural indicators for calcite decomposition such as the vesicular texture described in the dolomite grains were observed. Lack of evidence for calcium oxide (due to calcite decomposition) or portlandite (due to reaction of calcium oxide with water from room humidity) may suggest that the temperature in the DDZ was effectively buffered at 800 °C by the dolomite decarbonation reaction (Fig. 9), below the ca. 900 °C required to decarbonate calcite.

The dolomite grains with vesicular rims and recrystallized calcite matrix of the experimental samples (Figs. 7d, 10) show a remarkable similarity to the dolomite grains and calcite matrix microstructures found in the basal layer of the Heart Mountain landslide (Figs. 3d, 10). Anders et al. (2010) previously interpreted the calcite rich matrix in the basal layer as being a secondary cement precipitated from meteoric and hydrothermal fluids migrating up to and along the base of the slide block after cessation of slip. Our experiments suggest an alternative formation mechanism involving recrystallization and/or annealing of fine-grained calcite gouge due the high-temperatures attained during sliding. One can imagine a situation post-slip in which the porous decarbonated experimental grains may develop over time into microstructures resembling the natural dolomite grains with concentric calcite rims (Fig. 10a), where hydrothermal and meteoric fluids precipitate calcite within the vesicles. These vesicular textures have previously been interpreted as forming by dissolution over time to form skeletal grains, not dynamically, and then infilled by post-slip calcite and silica precipitation events related to hydrothermal and meteoric fluids identified by cathode luminescence and isotopic compositions (Anders et al., 2010).

We propose that thermal decomposition as evidenced by pervasive vesiculation textures, and the subsequent release of CO_2, indicate that temperatures in the slip zone locally reached the decomposition temperature of carbonates (at least 600 °C for dolomite; Rat'ko et al., 2011) within just a few hundred µm of slip. This near-instantaneous CO_2 production combined with porosity reduction during grain crushing drives local overpressure and reduces the effective stress on the sliding surface (Billi and Di Toro, 2008; Rowe et al., 2012; Sulem and Famin, 2009). While experimental constraints limited normal stresses to 10 MPa, at depths of 2–4 km the rate and amount of CO_2 produced would be significantly increased. Assuming a low permeability of the wallrock adjacent to the slip zone (Goren et al., 2010a, 2010b), once the slide was triggered the system may self-pressurize and promote slip from a very early stage. Prior to this stage other mechanisms must account for initiation of movement on a 2° slope (Aharonov and Anders, 2006; Hughes, 1970; Melosh, 1983). We suggest that the forsterite (Fig. 3) discovered in the natural samples was formed dynamically during the extreme frictional heating associated with slip by the reaction

$$2\ \text{dolomite} + \text{quartz} \rightarrow \text{forsterite} + 2\ \text{calcite} + 2\ CO_2.$$

Forsterite has been shown to form by the silicification of dolomite during contact metamorphism (Ferry et al., 2011) in the presence of SiO_2 and CO_2 rich fluids at temperatures of 655 °C and pressures of 50 MPa, equivalent to depth of the landslide basal surface.

Our experimental results compare favorably with theoretical calculations (Goren et al., 2010a, 2010b) and field observations made along the base of the Heart Mountain landslide (Anders et al., 2010; Craddock et al., 2012). The textures and chemical reactions we observed in the experiments suggest that the release of CO_2 gases by frictional heating of carbonates is a viable mechanism to explain catastrophic emplacement of landslides that move for large distances on low-angle surfaces.

Acknowledgements

Federico Zorzi is thanked for XRD analysis. Elena Spagnuolo and Marie Violay are thanked for assistance with high velocity experiments. Maureen McAuliffe Anders for help with graphics. We acknowledge funding by the European Research Council projects 205175 (USEMS) and 614705 (NOFEAR), and 2014 University of Otago Research Grant (to Smith). We thank Chris Scholz for comments on earlier versions of the manuscript. We thank Stephen Miller and two anonymous reviewers for their constructive reviews.

References

Aharonov, E., Anders, M.H., 2006. Hot water: a solution to the Heart Mountain detachment problem? Geology 34, 165–168.
Anders, M.H., Aharonov, E., Walsh, J.J., 2000. Stratified granular media beneath large slide blocks: implications for mode of emplacement. Geology 28, 971–974.
Anders, M.H., Craddock, J.P., Malone, D.H., Magloughlin, J.F., 2011. Heart Mountain and South Fork fault systems: architecture and evolution of the collapse of an Eocene volcanic system, northwest Wyoming: comment. Rocky Mt. Geol. 46, 71–75.
Anders, M.H., Fouke, B.W., Zerkle, A.L., Tavarnelli, E., Alvarez, W., Harlow, G.E., 2010. The role of calcining and basal fluidization in the long runout of carbonate slides: an example from the Heart Mountain slide block, Wyoming and Montana, USA. J. Geol. 118, 577–599.
Beeler, N.M., Tullis, T.E., Goldsby, D.L., 2008. Constitutive relationships and physical basis of fault strength due to flash heating. J. Geophys. Res., Solid Earth 113.
Beutner, E.C., Craven, A.E., 1996. Volcanic fluidization and the Heart Mountain detachment, Wyoming. Geology 24, 595–598.
Beutner, E.C., Gerbi, G.P., 2005. Catastrophic emplacement of the heart mountain block slide, Wyoming and Montana, USA. Geol. Soc. Am. Bull. 117, 724–735.

Beutner, E.C., Hauge, T.A., 2009. Heart Mountain and South Fork fault systems: architecture and evolution of the collapse of an Eocene volcanic system, northwest Wyoming. Rocky Mt. Geol. 44, 147–164.
Billi, A., Di Toro, G., 2008. Fault-related carbonate rocks and earthquake indicators: recent advances and future trends. In: Landowe, S.J., Hammler, G.M. (Eds.), Structural Geology: New Research. Nova Science Publishers, New York, ISBN 978-1-60456-827-1, pp. 63–86.
Brantut, N., Han, R., Shimamoto, T., Findling, N., Schubnel, A., 2011. Fast slip with inhibited temperature rise due to mineral dehydration: evidence from experiments on gypsum. Geology 39, 59–62.
Brian Dade, W., Huppert, H.E., 1998. Long-runout rockfalls. Geology 26, 803–806.
Bucher, W.H., 1947. Heart Mountain problem. In: Blackstone Jr., D.L., Sternberg, C.W. (Eds.), Field Conference Guidebook. Field Conference in the Bighorn Basin. Wyoming Geological Association.
Carslaw, H.S., Jaeger, J.C., 1959. Conduction of Heat in Solids, 2nd edition. Oxford University Press.
Collettini, C., Viti, C., Tesei, T., Mollo, S., 2013. Thermal decomposition along natural carbonate faults during earthquakes. Geology 41, 927–930.
Craddock, J.P., Geary, J., Malone, D.H., 2012. Vertical injectites of detachment carbonate ultracataclasite at White Mountain, Heart Mountain detachment, Wyoming. Geology 40, 463–466.
Craddock, J.P., Malone, D.H., Magloughlin, J., Cook, A.L., Rieser, M.E., Doyle, J.R., 2009. Dynamics of the emplacement of the Heart Mountain allochthon at White Mountain: constraints from calcite twinning strains, anisotropy of magnetic susceptibility, and thermodynamic calculations. Geol. Soc. Am. Bull. 121, 919–938.
Craddock, J.P., Nielson, K.J., Malone, D.H., 2000. Calcite twinning strain constraints on the emplacement rate and kinematic pattern of the upper plate of the Heart Mountain Detachment. J. Struct. Geol. 22, 983–991.
Dake, C.L., 1916. The Heart Mountain overthrust and associated structures in Park County, Wyoming. J. Geol. 26, 45–55.
De Paola, N., Chiodini, G., Hirose, T., Cardellini, C., Caliro, S., Shimamoto, T., 2011a. The geochemical signature caused by earthquake propagation in carbonate-hosted faults. Earth Planet. Sci. Lett. 310, 225–232.
De Paola, N., Hirose, T., Mitchell, T., Di Toro, G., Viti, C., Shimamoto, T., 2011b. Fault lubrication and earthquake propagation in thermally unstable rocks. Geology 39, 35–38.
Deegan, F.M., Troll, V.R., Freda, C., Misiti, V., Chadwick, J.P., McLeod, C.L., Davidson, J.P., 2010. Magma–carbonate interaction processes and associated CO_2 release at Merapi Volcano, Indonesia: insights from experimental petrology. J. Petrol. 51, 1027–1051.
Di Toro, G., Han, R., Hirose, T., De Paola, N., Nielsen, S., Mizoguchi, K., Ferri, F., Cocco, M., Shimamoto, T., 2011. Fault lubrication during earthquakes. Nature 471, 494.
Di Toro, G., Niemeijer, A., Tripoli, A., Nielsen, S., Di Felice, F., Scarlato, P., Spada, G., Alessandroni, R., Romeo, G., Di Stefano, G., Smith, S., Spagnuolo, E., Mariano, S., 2010. From field geology to earthquake simulation: a new state-of-the-art tool to investigate rock friction during the seismic cycle (SHIVA). Rend. Lincei, Sci. Fis. Nat. 21, 95–114.
Ferry, J.M., Ushikubo, T., Valley, J.W., 2011. Formation of forsterite by silicification of dolomite during contact metamorphism. J. Petrol. 52, 1619–1640.
Fondriest, M., Smith, S.A.F., Candela, T., Nielsen, S.B., Mair, K., Di Toro, G., 2013. Mirror-like faults and power dissipation during earthquakes. Geology 41, 1175–1178.
Goldsby, D.L., Tullis, T.E., 2011. Flash heating leads to low frictional strength of crustal rocks at earthquake slip rates. Science 334, 216–218.
Goren, L., Aharonov, E., Anders, M.H., 2010a. Thermo–poro–mechanical effects in landslide mechanics. In: Hafzor, Y.H., Sulem, J., Vardoulakis, I. (Eds.), Meso-scale Shear Physics in Earthquakes and Landslides, pp. 255–274.
Goren, L., Aharonov, E., Anders, M.H., 2010b. The long runout of the Heart Mountain landslide: heating, pressurization, and carbonate decomposition. J. Geophys. Res., Solid Earth 115 (B10), B10210. http://dx.doi.org/10.1029/2009JB007113.
Han, R., Shimamoto, T., Hirose, T., Ree, J.H., Ando, J., 2007a. Ultralow friction of carbonate faults caused by thermal decomposition. Science 316, 878–881.
Han, R.H., Shimamoto, T., Ando, J.I., Ree, J.H., 2007b. Seismic slip record in carbonate-bearing fault zones: an insight from high-velocity friction experiments on siderite gouge. Geology 35, 1131–1134.
Hauge, T.A., 1985. Gravity-spreading origin of the Heart Mountain allochthon, northwestern Wyoming. Geol. Soc. Am. Bull. 96, 1440–1456.
Hauge, T.A., 1990. Kinematic model of a continuous Heart Mountain allochthon. Geol. Soc. Am. Bull. 102, 1174–1188.
Hauge, T.A., 1993. The Heart Mountain detachment, northwestern Wyoming; 100 years of controversy. In: Snoke, A.W., Steidtmann, J.R., Roberts, S.M. (Eds.), Geology of Wyoming: Memoir. Geological Survey of Wyoming, Laramie, WY, pp. 530–571.
Herwegh, M., Berger, A., Ebert, A., Brodhag, S., 2008. Discrimination of annealed and dynamic fabrics: consequences for strain localization and deformation episodes of large-scale shear zones. Earth Planet. Sci. Lett. 276, 52–61.
Hughes, C.J., 1970. The Heart Mountain detachment fault—a volcanic phenomenon? J. Geol. 78, 107–116.
Logan, J.M., Friedman, M., Higgs, N., Dengo, C., Shimamoto, T., 1979. Experimental studies of simulated gouge and their application to studies of natural fault zones. In: Proceedings of Conference VIII on Analysis of Actual Fault Zones in Bedrock. U.S. Geological Survey Open-File Report, p. 79-1239.
Malone, D.H., Craddock, J.P., Anders, M.H., Wulff, A., 2014. Constraints on the emplacement age of the massive Heart Mountain slide, northwestern Wyoming. J. Geol. 122 (6), 1–15.
Melosh, H.J., 1983. Acoustic fluidization: can sound waves explain why dry rock debris appears to flow like a fluid in some energetic geologic events? Am. Sci. 71, 158–165.
Pierce, W.G., 1960. The "break-away" point on the Heart Mountain detachment fault in northwestern Wyoming. In: U.S. Geol. Surv. Prof. Paper, vol. 400B, pp. 236–237.
Pierce, W.G., 1973. Principal features of the Heart Mountain fault, and the mechanism problem. In: DeJong, K.A., Scholten, R. (Eds.), Gravity and Tectonics. John Wiley and Sons, New York, pp. 457–471.
Proctor, B.P., Mitchell, T.M., Hirth, G., Goldsby, D., Zorzi, F., Platt, J.D., Di Toro, G., 2014. Dynamic weakening of serpentinite gouges and bare-surfaces at seismic slip rates. J. Geophys. Res., Solid Earth. http://dx.doi.org/10.1002/2014JB011057.
Pudasaini, S.P., Miller, S.A., 2013. The hypermobility of huge landslides and avalanches. Eng. Geol. 157, 124–132.
Rat'ko, A.I., Ivanets, A.I., Kulak, A.I., Morozov, E.A., Sakhar, I.O., 2011. Thermal decomposition of natural dolomite. Inorg. Mater. 47, 1372–1377.
Rice, J.R., 2006. Heating and weakening of faults during earthquake slip. J. Geophys. Res., Solid Earth 111.
Rowe, C.D., Fagereng, A., Miller, J.A., Mapani, B., 2012. Signature of coseismic decarbonation in dolomitic fault rocks of the Naukluft Thrust, Namibia. Earth Planet. Sci. Lett. 333, 200–210.
Smith, S.A.F., Di Toro, G., Kim, S., Ree, J.H., Nielsen, S., Billi, A., Spiess, R., 2013. Coseismic recrystallization during shallow earthquake slip. Geology 41, 63–66.
Sulem, J., Famin, V., 2009. Thermal decomposition of carbonates in fault zones: slip-weakening and temperature-limiting effects. J. Geophys. Res., Solid Earth 114.
Tisato, N., Di Toro, G., De Rossi, N., Quaresimin, M., Candela, T., 2012. Experimental investigation of flash weakening in limestone. J. Struct. Geol. 38, 183–199.
Violay, M., Nielsen, S., Spagnuolo, E., Cinti, D., Di Toro, G., Di Stefano, G., 2013. Pore fluid in experimental calcite-bearing faults: abrupt weakening and geochemical signature of co-seismic processes. Earth Planet. Sci. Lett. 361, 74–84.
Voight, B., 1973. The mechanics of retrogressive block-gliding, with emphasis on the evolution of the Turnagain Heights landslide, Anchorage, Alaska. In: DeJong, K.A., Scholten, R. (Eds.), Gravity and Tectonics. John Wiley and Sons, New York, pp. 97–121.